

Magnetoresistance in bilayer graphene via ferromagnet proximity effects

Y. G. Semenov, J. M. Zavada, and K. W. Kim

*Department of Electrical and Computer Engineering,
North Carolina State University, Raleigh, NC 27695-7911*

Abstract

A drastic modification of electronic band structure leading to the magnetoresistance is predicted in bilayer graphene when it is placed between two ferromagnetic insulators. Due to the exchange interaction with the proximate ferromagnet, the electronic energy dispersion in the graphene channel strongly depends on the magnetization orientation of two ferromagnetic layers, \mathbf{M}_1 and \mathbf{M}_2 . While the parallel configuration $\mathbf{M}_1 = \mathbf{M}_2$ leads to simple spin splitting of both conduction and valence bands, an energy gap is induced as soon as the angle θ between \mathbf{M}_1 and \mathbf{M}_2 becomes non-zero with the maximum achieved at $\theta = \pi$ (i.e., antiparallel alignment). Consequently, bilayer graphene may exhibit a sizable magnetoresistance effect in the current-in-plane configuration. A rough estimate suggests that the resistance change on the order of tens of percent is possible at room temperature. This effect is expected to become more pronounced as the temperatures decreases.

PACS numbers: 73.21.-b, 85.75.-d, 73.43.Qt, 73.61.Wp

With the advent of free-standing atomically thin graphite films (or graphene),¹ unusual properties related to the two-dimensional Dirac-like relativistic spectrum of the honeycomb carbon lattice² put graphene in the forefront of emerging carbon based electronics. Among others, the half-integer quantum Hall effect^{3,4,5} observed even at room temperature,⁶ high carrier mobility, easy control of electron and hole concentrations via variation of applied bias, absence of weak localization and universal minimal conductivity at the Dirac point with zero density of states have attracted significant theoretical and experimental attention to electronic transport in graphene.^{7,8,9}

The spin dependent properties of graphene also offer fascinating opportunities. In most studies, the starting point of consideration is its extremely small spin-orbital coupling compared to typical semiconductors.^{10,11} Consequently, graphene exhibits long electron spin-relaxation time¹² and mean free paths^{13,14} even at room temperature.¹⁵ However, this very advantage (i.e., the weak spin-orbital interaction) presents a severe challenge in spin manipulation or selection via electrical control. One possible approach may be to utilize the electron exchange interaction with proximate ferromagnetic layers and the resulting effective magnetic field.^{16,17}

It was found very recently that bilayer graphene (BLG) offers a host of novel phenomena through external modification of the energy band structure.^{18,19,20,21,22} Particularly, it was shown that a gap opens up between the conduction and valence energy bands when a potential difference u is introduced in the two graphene layers. Moreover, the parabolic band structure near the non-equivalent K and K' points²³ transforms to a Mexican-hat-like dispersion with $u \neq 0$.¹⁹ Likewise, a non-trivial response may be expected in BLG to the symmetry-breaking *spin-dependent* interactions.

In this study, the properties of BLG sandwiched between two insulating/dielectric ferromagnets with magnetic moments \mathbf{M}_1 and \mathbf{M}_2 are exploited based on an 8×8 tight-binding model. Similar to the electrical bias, the calculation predicts a significant modification of the electronic band structure when the constituting graphene layers are subject to un-equal exchange interactions with the proximate magnetic ions. A particularly interesting feature appears for ferromagnetic layers with identical magnitude of the magnetic moments ($M_1 = M_2$), where $u = 0$ and the *potential asymmetry* is not a factor. As the alignment of \mathbf{M}_1 and \mathbf{M}_2 deviates from each other, the spin interactions reveal an asymmetry that can alter the BLG energy bands (including an energy gap) and subsequently the in-plane con-

ductivity. The resulting magnetoresistance effect can play an important role in the carbon based spintronics. In the case of monolayer graphene, on the other hand, the net effect of two magnetic layers simply reduces to electron spin splitting in the effective field induced by the vectorial sum $\mathbf{M}_1 + \mathbf{M}_2$.

Figure 1 schematically illustrates the specific structure under consideration. It resembles the ferromagnet-metal hybrid structures²⁴ that reveal a giant magnetoresistance owing to the spin-dependent conductivity. The bottom ferromagnetic dielectric layer (FDL) possesses the magnetization \mathbf{M}_1 that can be pinned along the direction of the x axis by an antiferromagnetic substrate. The top FDL may be constructed from the same material but its magnetization vector \mathbf{M}_2 can be rotated on the x - y plane (by an external magnetic field) forming an angle θ with \mathbf{M}_1 . The influence of FDL magnetization on BLG electronic structure can be realized in actual structures through either the direct exchange interaction with magnetic ions (assuming an overlap between the carbon π -orbitals and unfilled shells of the magnetic ions in FDLs) or an indirect interaction via the ligands of FDLs. Thus, the problem can be modeled in the mean field approximation with the Hamiltonian

$$H = H_{BL} + \mathcal{P}_1 \alpha \mathbf{M}_1 \mathbf{S} + \mathcal{P}_2 \alpha \mathbf{M}_2 \mathbf{S}, \quad (1)$$

where H_{BL} is the spin-independent BLG Hamiltonian. Two remaining terms of Eq. (1) describe the energy of an electron spin \mathbf{S} in the effective fields (in units of energy) $\alpha \mathbf{M}_1$ and $\alpha \mathbf{M}_2$ of the proximate FDLs. Accordingly, projection operator \mathcal{P}_1 (\mathcal{P}_2) is 1 for the electron localized at the bottom (top) carbon monolayer and 0 otherwise. Parameter α is proportional to the carrier-ion exchange constant as evaluated in Refs. 16 and 17.

In the case of low energy electronic excitations, the tight-binding approximation¹⁹ can accurately describe the BLG band spectra as recently demonstrated in a density functional calculation.²¹ Hence, we adopt the tight-binding Hamiltonian near the valley extrema in a basis that constitutes the components $(A_1 \uparrow, A_1 \downarrow, B_2 \uparrow, B_2 \downarrow, A_2 \uparrow, A_2 \downarrow, B_1 \uparrow, B_1 \downarrow)$ for the K valley and $(B_2 \uparrow, B_2 \downarrow, A_1 \uparrow, A_1 \downarrow, B_1 \uparrow, B_1 \downarrow, A_2 \uparrow, A_2 \downarrow)$ for the K' valley. Here, A_i and B_i correspond to the electron amplitudes at inequivalent sites of the bottom ($i = 1$) and top ($i = 2$) graphene layers as shown in Fig. 1(b), and \uparrow and \downarrow denote spin up and spin down states.

The Hamiltonian H_{BL} includes the lateral coupling for nearest carbon atoms in the bottom $(A_1 - B_1)$ and top $(A_2 - B_2)$ layers with the matrix element γ ($= 3$ eV) as well as the

interlayer coupling for $A_2 - B_1$ and $A_1 - B_2$ dimers with the matrix elements γ_1 ($= 0.4$ eV) and γ_3 ($= 0.3$ eV), respectively; hence, $\gamma_3 < \gamma_1 \ll \gamma$. At zero magnetic field, Eq. (1) for the lowest electronic states in the K and K' valleys can be expressed in terms of the in-plane electron momentum $\mathbf{k} = (k_x, k_y)$ defined from the centrum of each valley as

$$H_{\varkappa} = \varkappa \begin{pmatrix} -\frac{1}{2}u & \frac{\varkappa}{2}\alpha M_{\varkappa} & v_3 k e^{i\varphi} & 0 & 0 & 0 & v k e^{-i\varphi} & 0 \\ \frac{\varkappa}{2}\alpha M_{\varkappa}^* & -\frac{1}{2}u & 0 & v_3 k e^{i\varphi} & 0 & 0 & 0 & v k e^{-i\varphi} \\ v_3 k e^{-i\varphi} & 0 & \frac{1}{2}u & \frac{\varkappa}{2}\alpha M_{-\varkappa} & v k e^{i\varphi} & 0 & 0 & 0 \\ 0 & v_3 k e^{-i\varphi} & \frac{\varkappa}{2}\alpha M_{-\varkappa}^* & \frac{1}{2}u & 0 & v k e^{i\varphi} & 0 & 0 \\ 0 & 0 & v k e^{-i\varphi} & 0 & \frac{1}{2}u & \frac{\varkappa}{2}\alpha M_{-\varkappa} & \varkappa \gamma_1 & 0 \\ 0 & 0 & 0 & v k e^{-i\varphi} & \frac{\varkappa}{2}\alpha M_{-\varkappa}^* & \frac{1}{2}u & 0 & \varkappa \gamma_1 \\ v k e^{i\varphi} & 0 & 0 & 0 & \varkappa \gamma_1 & 0 & -\frac{1}{2}u & \frac{\varkappa}{2}\alpha M_{\varkappa} \\ 0 & v k e^{i\varphi} & 0 & 0 & 0 & \varkappa \gamma_1 & \frac{\varkappa}{2}\alpha M_{\varkappa}^* & -\frac{1}{2}u \end{pmatrix}, \quad (2)$$

where the index \varkappa separates the case of K ($\varkappa = +1$) and K' ($\varkappa = -1$) valleys, $\varphi = \tan^{-1}(k_y/k_x)$, $M_{+1} = M_1$, $M_{-1} = M_2 e^{-i\theta}$, and $v = \sqrt{3}a\gamma/2\hbar$ is the electron velocity at the Fermi energy in monolayer graphene.³ In addition, the term $v_3 = \sqrt{3}a\gamma_3/2\hbar$ ($\ll v$) is responsible for the trigonal warping, where $a = 0.249$ nm is the length of lattice unit vector. The secular equation for Eq. (2) is solved under the conditions of (i) zero bias and (ii) identical top and bottom FM materials (i.e., $u = 0$, $M_1 = M_2 \equiv M$). For simplicity, the transfer matrix elements for off-center sites A_1 and B_2 are also ignored ($v_3 \rightarrow 0$). This approximation does not change qualitatively the results for the energies $E > 1$ meV as discussed in Ref. 22.

The specified conditions leads to the energy spectra of each valley consisting of eight non-degenerate branches $\varepsilon_n(k)$ that are identical for conduction and valence bands and isotropic with respect to the valley centrum (i.e., independent of φ). Two spin pair solutions correspond to the excited states with energies $|\varepsilon_n(k)| \gtrsim \gamma_1$ that are beyond the current interest. Hence, only the remaining four low-energy bands $\varepsilon_n = \varepsilon_n(k)$ are considered. As it is convenient to normalize the parameters in units of γ_1 , the dimensionless momentum $p \equiv vk/\gamma_1$ and the exchange field $\mathbf{G} \equiv \alpha\mathbf{M}/\gamma_1$ are introduced hereinafter. The low energy bands $\varepsilon_n = \pm\gamma_1 E_{\pm}$ can be expressed as

$$E_{\pm} = \sqrt{p^2 + \frac{G^2}{4} + \frac{1}{2} \left(1 \pm G \cos \frac{\theta}{2} - W_{\pm} \right)}, \quad (3)$$

where

$$W_{\pm} = \sqrt{\left(1 \pm G \cos \frac{\theta}{2}\right)^2 (1 + 4p^2) + 2p^2 G^2 (1 - \cos \theta)} \quad (4)$$

for $0 \leq \theta \leq \pi$. Two solutions with $\varepsilon_n > 0$ correspond to the lowest conduction bands, while their mirror images with respect to the zero energy describe the highest valence bands.

The most remarkable outcome of the calculation is the presence of an energy gap E_g between the lowest conduction band and the highest valence band for $\theta \neq 0$ as shown in Fig. 2. When the orientation of \mathbf{M}_1 and \mathbf{M}_2 is in parallel alignment [$\theta = 0$, Fig. 2(a)], the net effect of the exchange interaction simply lifts the two-fold spin degeneracy resulting in two pairs of spin-split bands that cross each other at $p = \sqrt{G(1 + G/2)}/2$. However, once they are disaligned, the electronic bands become of mixed spin character (e.g., with both parallel and antiparallel components to the x direction). Subsequent anti-crossing opens up the gap that progressively grows with θ . At $\theta = \pi$ [i.e., $\mathbf{M}_1 = -\mathbf{M}_2$, Fig. 2(d)], the conduction and valence bands are merged to form two doubly degenerate states with the maximal $E_g = G/\sqrt{1 + G^2}$ at $p = G\sqrt{2 + G^2}/2\sqrt{1 + G^2}$. This spin degeneracy is not surprising because the equivalence of top and bottom graphene layers makes the \mathbf{M}_1 and \mathbf{M}_2 ($= -\mathbf{M}_1$) directions indistinguishable [i.e., the dependence of Eqs. (3) and (4) on sign in $\pm G$ disappears]. Note that in the case of monolayer graphene, the effect of two FDLs in a similar configuration $\mathbf{M}_2 = -\mathbf{M}_1$ gives rise to net cancellation of spin-dependent band modification.

In general, the bandgap induced in BLG can be expressed in term of the deviation angle θ as

$$E_g = \frac{G \sin \theta/2}{\sqrt{1 + G^2 + 2G \cos \theta/2}}. \quad (5)$$

Evident from this equation, the strength of the effective field G determines the size of E_g . If its magnitude is comparable to the thermal energy (strictly speaking $\gamma_1 G \gtrsim k_B T$ as G is a normalized quantity), the orientation dependence in Eq. (5) may manifest itself through the variation of electron/hole population. At the same time, the carrier velocity in BLG is also strongly affected as indicated by the flattening of the bands with increasing θ in Fig. 2. Clearly the conductivity in the BLG channel can be modulated by the effective fields from the two ferromagnetic barriers, leading to a sizable magnetoresistance effect in the current-in-plane configuration.

The effect of both conduction/valence band separation and deformation on the magne-

toresistance $R(\theta)$ can be taken into account in the one-electron approximation in terms of Kubo-Greenwood formula for conductivity^{25,26}

$$\sigma_{xx} = (2\pi e)^2 \hbar \sum_{m,n} \sum_{\mathbf{k},\mathbf{k}'} |\langle m, \mathbf{k} | v_x | n, \mathbf{k}' \rangle|^2 \left(-\frac{\partial f}{\partial \varepsilon} \right)_{m,\mathbf{k}} \delta(\varepsilon_{m,\mathbf{k}} - \varepsilon_{n,\mathbf{k}'}), \quad (6)$$

where e is the electron charge, m and n the subband indices, $v_x = dx/dt = i[H_{\mathbf{x}}, x]/\hbar$ the velocity operator, and f the Fermi-Dirac function. The case of ballistic conductivity is examined at finite temperature.²⁷ The specific property of interest is the relative change $\sigma_{xx}(\theta)/\sigma_{xx}(0)$ as a function of θ . Utilizing $G \ll 1$ in most cases, our analysis reveals that it depends most sensitively on a single parameter $\gamma_1 G/k_B T$ as expected. Figure 3 provides the calculated $\sigma_{xx}(\theta)/\sigma_{xx}(0)$ as well as the corresponding change in the electron/hole concentration $n(\theta)/n(0)$ for two different values of $\gamma_1 G/k_B T$. The comparatively weaker decrease of n (in reference to σ_{xx}) as θ rotates signifies a major contribution of the mobility variation due to the flattened band structure.

Assuming a sensitive response of \mathbf{M}_2 to the external magnetic field, one can define the magnetoresistance as a difference of the BLG resistance $R(0) \sim 1/\sigma_{xx}(0)$ at $\mathbf{M}_1 = \mathbf{M}_2$ and $R(\pi) \sim 1/\sigma_{xx}(\pi)$ at $\mathbf{M}_1 = -\mathbf{M}_2$. Figure 4 presents the normalized result $\xi = [R(\pi) - R(0)]/R(0)$ as a function of $\gamma_1 G/k_B T$. Since this quantity depends on the position of the electro-chemical potential μ as well, four different values of $|\mu|/k_B T$ are considered. All the cases show essentially the same characteristics with the largest effect exhibited at $\mu = 0$ (i.e., μ at the mid gap). ξ also saturates at smaller effective fields as μ gets closer to the conduction/valence band edge. An important point to note is that the magnetoresistance effect of *tens of percent* is possible once the exchange field strength $\gamma_1 G$ ($\equiv \alpha M$) is comparable to the thermal energy. By comparison, the alternative approach based on spin-valve devices in monolayer graphene reveals only a feeble magnetoresistance due to the weak dependence of the graphene conductivity on the electronic details of the ferromagnetic leads.²⁸

As a practical matter, the strength of the exchange field G is of major importance. Considering a large variety of potential FDL/graphene interfaces and the current lack of relevant information, however, *a priori* evaluation of G may be possible only in a very rough manner. Following the approach presented in Ref. 17, we estimate the exchange energy for a graphene electron interacting with the nearest stratum of magnetic ions as $\alpha M = (n_{2FM}/n_{2C})S_M J$, where n_{2C} and n_{2FM} are the areal concentrations of graphene carbon atoms

and magnetic ions in the FDL, respectively, S_M is the mean value of the magnetic ion spins, and J is the exchange constant. The latter was found to be $J = 15$ meV as deduced from an experiment in an EuO/Al structure with Curie temperature $T_c = 69$ K.²⁹ This constant J may actually be larger in the case of high temperature ferromagnets with stronger spin-spin inter-ions interaction. With the provision that $J \sim T_c$, $n_{2FM}/n_{2C} = 0.1 - 0.2$, $S_M = 1 - 2.5$ and $T_c = 500 - 600$ K, we find $\gamma_1 G (\equiv \alpha M) \simeq 15 - 65$ meV. Although the accuracy of this estimate is limited, it nonetheless shows the possibility of prominent magnetoresistance effect even at room temperature. Lower temperatures will make its manifestation far more apparent for easier detection.

It is noted that the idealized model of Eq. (1) may need to be expanded for detailed analysis of a specific structure. Imperfect interfaces between the FDL and BLG can be a source of a random potential that affects the electronic band structure and transport properties of graphene.³⁰ In addition, any difference between the top and bottom FDLs results in a non-zero bandgap even at parallel orientation of their magnetic moments. At the same time, the non-trivial manifestation of electron-electron interaction^{31,32} may interplay with the studied effects at sufficiently low temperatures. These factors (and many others)⁹ may need to be taken into consideration as the situation requires.

This work was supported in part by the US Army Research Office and the FCRP Center on Functional Engineered Nano Architectonics (FENA).

-
- ¹ K. S. Novoselov *et al.*, Science **306**, 666 (2004).
 - ² G. W. Semenoff, Phys. Rev. Lett. **53**, 2449 (1984).
 - ³ K. S. Novoselov *et al.*, Nature (London) **438**, 197 (2005).
 - ⁴ Y. Zhang *et al.*, Nature (London) **438**, 201 (2005).
 - ⁵ V. P. Gusynov and S. G. Sharapov, Phys. Rev. Lett. **95**, 146801 (2005).
 - ⁶ K. S. Novoselov *et al.*, Science **315**, 1379 (2007).
 - ⁷ A. K. Geim and K. S. Novoselov, Nat. Mater. **6**, 183 (2007).
 - ⁸ V. I. Fal'ko, and A. K. Geim, Eur. Phys. J. **148**, 1 (2007).
 - ⁹ A. H. Castro Neto *et al.*, arXiv:cond-mat/0709.1163 (unpublished).
 - ¹⁰ H. Min *et al.*, Phys. Rev. B **74**, 165310 (2006).
 - ¹¹ D. Huertas-Hernando, F. Guinea and A. Brataas, Phys. Rev. B **74**, 155426 (2006).
 - ¹² D. Huertas-Hernando, F. Guinea, and A. Brataas, Eur. Phys. J. **148**, 177 (2007).
 - ¹³ B. Oezylmaz and P. Kim, in *Final Program of the 2007 Electronic Materials Conference* (South Bend, Indiana, 2007), Vol. 1, p. 85.
 - ¹⁴ S. Cho, Y.-Fu Chen, and M. S. Fuhrer, Appl. Phys. Lett. **91**, 123105 (2007).
 - ¹⁵ N. Tombros *et al.*, Nature (London) **448**, 571 (2007).
 - ¹⁶ Y. G. Semenov, K. W. Kim, and J. Zavada, Appl. Phys. Lett. **91**, 153105 (2007).
 - ¹⁷ H. Haugen, D. Huertas-Hernando, and A. Brataas, arXiv:cond-mat/0707.3976 (unpublished).
 - ¹⁸ K. S. Novoselov *et al.*, Nat. Phys. **2**, 177 (2006).
 - ¹⁹ E. McCann and V. I. Fal'ko, Phys. Rev. Lett. **96**, 086805 (2006).
 - ²⁰ E. V. Castro *et al.*, Phys. Rev. Lett. **99**, 216802 (2007).
 - ²¹ H. Min *et al.*, Phys. Rev. B **75**, 155115 (2007).
 - ²² E. McCann, D. S. L. Abergel, and V. I. Fal'ko, Eur. Phys. J. **148**, 91 (2007).
 - ²³ M. S. Dresselhouse and D. Dresselhouse, Adv. Phys. **51**, 1 (2002).
 - ²⁴ See, for example, M. N. Baibich *et al.*, Phys. Rev. Lett. **61**, 2472 (1988).
 - ²⁵ R. Kubo, J. Phys. Soc. Japan **12**, 570 (1957).
 - ²⁶ D. A. Greenwood, Proc. Phys. Soc. **71**, 585 (1958).
 - ²⁷ The conductance of graphene subjected to a random potential was evaluated in terms of the Kubo-Greenwood formula by K. Nomura, M. Koshino, and S. Ryu, Phys. Rev. Lett. **99**, 146806

(2007).

- ²⁸ L. Brey and H. A. Fertig, Phys. Rev. B **76**, 205435 (2007).
- ²⁹ G. M. Roesler *et al.*, Proc. SPIE **2157**, 285 (1994).
- ³⁰ J. Nilsson *et al.*, arXiv:cond-mat/0712.3259 (unpublished).
- ³¹ E. V. Castro *et al.*, arXiv:cond-mat/0711.0758 (unpublished).
- ³² J. Nilsson *et al.*, Phys. Rev. B **73**, 214418 (2006).

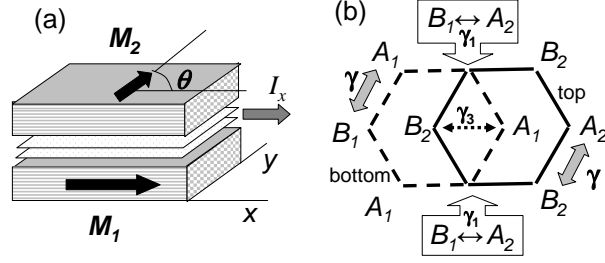


FIG. 1: (a) Schematic illustration of bilayer graphene (two closely set planes) sandwiched between ferromagnetic dielectric layers of magnetization \mathbf{M}_1 and \mathbf{M}_2 (separated by the angle θ). The reference frame is chosen so that \mathbf{M}_1 is along the x axis; the grey arrow shows the probing current I_x through the graphene channel. (b) Fragment of bilayer graphene as two hexagons (view from above) with carbon atoms located at the vertices. Lattice sites A_1 and B_1 (dashed hexagon) refer to the bottom layer, while A_2 and B_2 (solid hexagon) the top layer. γ , γ_1 , and γ_3 represent the matrix elements for electron transfer between the nearest in-plane, vertical, and slanted inter-layer carbon atoms, respectively.

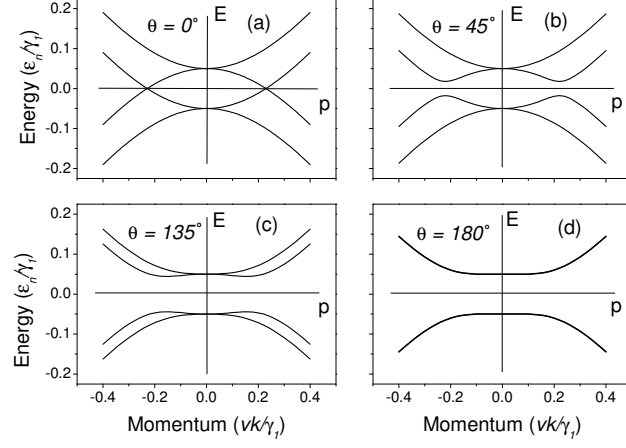


FIG. 2: Electron energy spectra of bilayer graphene near the K point at different angles θ between magnetization vectors \mathbf{M}_1 and \mathbf{M}_2 . The reference for energy $E = 0$ corresponds to the center of the bandgap [(b)-(d)] or the point of contact between the conduction and valence bands in the case $\theta = 0$ [(a)]. The bands are doubly degenerate at $\theta = \pi$ [(d)].

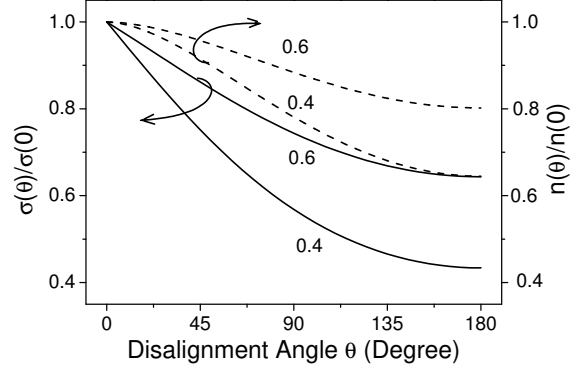


FIG. 3: Conductivity σ (solid lines) and carrier concentration n (dashed lines) vs. θ in bilayer graphene at two different ratios of the thermal energy $k_B T$ to the exchange field $\gamma_1 G$ (i.e., $k_B T / \gamma_1 G = 0.6$ or 0.4). The electro-chemical potential is fixed at zero (i.e., at the middle of the energy gap).

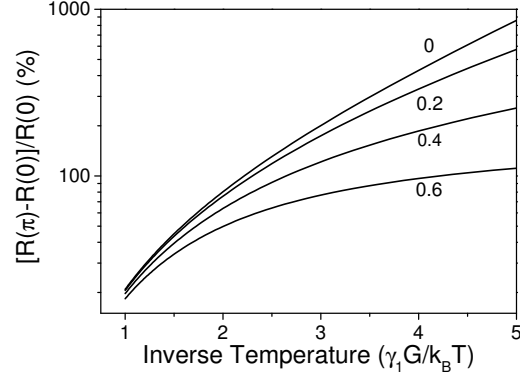


FIG. 4: Magnetoresistance ξ in the anti-parallel alignment ($\mathbf{M}_1 = -\mathbf{M}_2$) as a function of $\gamma_1 G / k_B T$ calculated at different locations of the electro-chemical potential μ . The normalized value $\mu / k_B T$ is provided for each curve.